JACS
JOURNAL OF THE AMERICAN CHEMICAL SOCIETY
Article
pubs.acs.org/JACS

High-Yield Exfoliation of Ultrathin Two-Dimensional Ternary Chalcogenide Nanosheets for Highly Sensitive and Selective Fluorescence DNA Sensors

Chaoliang Tan,[†,⊥] Peng Yu,[†,⊥] Yanling Hu,[†,‡,⊥] Junze Chen,[†] Ying Huang,[†] Yongqing Cai,[§] Zhimin Luo,[†] Bing Li,[∥] Qipeng Lu,[†] Lianhui Wang,*[,‡] Zheng Liu,*[,†] and Hua Zhang*[,†]

[†]School of Materials Science and Engineering, Nanyang Technological University, 50 Nanyang Avenue, Singapore 639798, Singapore

[‡]Key Laboratory for Organic Electronics and Information Display (KLOEID) and Institute of Advanced Materials (IAM), Jiangsu National Synergetic Innovation Center for Advanced Materials (SICAM) Nanjing University of Posts and Telecommunications, 9 Wenyuan Road, Nanjing 210046, China

[§]Institute of High Performance Computing, A*STAR (Agency for Science, Technology and Research) 1 Fusionopolis Way, Singapore 138632, Singapore

[∥]Institute of Materials Research and Engineering, A*STAR (Agency for Science, Technology and Research), 3 Research Link, Singapore 117602, Singapore

Supporting Information

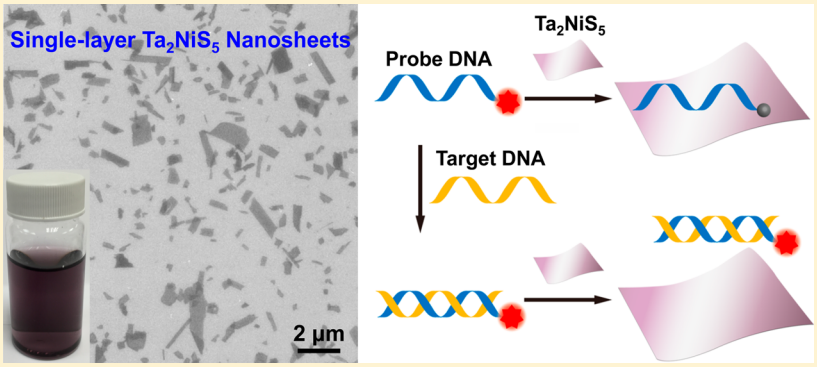

ABSTRACT: High-yield preparation of ultrathin two-dimensional (2D) nanosheets is of great importance for the further exploration of their unique properties and promising applications. Herein, for the first time, the high-yield and scalable production of ultrathin 2D ternary chalcogenide nanosheets, including Ta_2NiS_5 and Ta_2NiSe_5, in solution is achieved by exfoliating their layered microflakes. The size of resulting Ta_2NiS_5 and Ta_2NiS_5 nanosheets ranges from tens of nanometers to few micrometers. Importantly, the production yield of single-layer Ta_2NiS_5 nanosheets is very high, ca. 86%. As a proof-of-concept application, the single-layer Ta_2NiS_5 is used as a novel fluorescence sensing platform for the detection of DNA with excellent selectivity and high sensitivity (with detection limit of 50 pM). These solution-processable, high-yield, large-amount ternary chalcogenide nanosheets may also have potential applications in electrocatalysis, supercapacitors, and electronic devices.

INTRODUCTION

Single- and few-layer transition metal dichalcogenide (TMD) nanosheets, such as MoS_2, TiS_2, TaS_2, WS_2, $MoSe_2$, etc., have been intensively studied over the past few years.[1−5] Due to their ultrathin two-dimensional (2D) geometry and the electron confinement in two dimensions, TMD nanosheets exhibited some unprecedented physical, chemical and electronic properties,[1−5] and showed great promises in various applications in electronic/optoelectronic devices,[6−10] catalysis,[11−13] sensors,[14−17] energy storage,[18−20] and biomedicines.[21,22] It is worth pointing out that the physical, chemical and electronic properties of layered TMD nanosheets are versatile and material-dependent, making each of them favorable for specific applications.[1,2] Therefore, it can be anticipated that the exploration of new members in the family of ultrathin 2D nanosheets of layered metal chalcogenides may bring some novel interesting properties, fascinating functions and promising applications.

Driven by their unique properties and wide potential applications, great research efforts have been devoted into developing various types of effective synthetic methods for preparation of ultrathin 2D TMD nanosheets.[1,2] Due to the weak interlayer interaction of layered TMDs, the single- or few-layer TMD nanosheets can be prepared by means of exfoliation methods, such as mechanical exfoliation,[23] liquid exfoliation,[24]

Received: July 6, 2015
Published: August 4, 2015

DOI: 10.1021/jacs.5b06982
J. Am. Chem. Soc. 2015, 137, 10430−10436

surfactant/polymer-assisted exfoliation,[25,26] Li/Na-intercalation and exfoliation,[27,28] and electrochemical Li-intercalation and exfoliation method.[29,30] Among them, the last method mentioned above, which was developed by our group, allows for the production of single-layer or few-layer metal chalcogenide nanosheets, such as MoS_2, WS_2, TaS_2, TiS_2, WSe_2, $NbSe_2$, Sb_2Se_3, and graphene in high yield and large amount at room temperature.[31,32] It is believed that this method can also be used for exfoliation of other TMDs to obtain the ultrathin 2D nanosheets.

In this contribution, for the first time, we present the high-yield and scalable preparation of ultrathin 2D ternary chalcogenide nanosheets, including Ta_2NiS_5 and Ta_2NiSe_5, in solution from their layered microflakes via our electrochemical Li-intercalation and exfoliation method. The Ta_2NiS_5 and Ta_2NiSe_5 layered microflakes are first prepared by the chemical vapor transport method from their elementary powders. After exfoliation, the yield of obtained single-layer Ta_2NiS_5 nanosheets is ca. 86%, but the obtained Ta_2NiSe_5 nanosheets are 2–5 layers. Importantly, the single-layer Ta_2NiS_5 nanosheet exhibits high fluorescence quenching ability. As a proof-of-concept application, fluorescent sensors based on single-layer Ta_2NiS_5 nanosheets are developed for the detection of DNA, which exhibit low detection limit (50 pM) and excellent selectivity.

RESULTS AND DISCUSSION

Ta_2NiS_2 and Ta_2NiSe_2 are both layered compounds,[31] which crystallize in the orthorhombic and monoclinic space group *Cmcm* (63) and *C*2/*c* (15), respectively. The structure of Ta_2NiQ_5 (Q = S, Se) characterizes the zigzag waved 2D layer (Figure 1a,b) consisting of the NiQ_4 tetrahedral single chains that are interconnected on both sides by the $[TaQ_6]_2$ dimer chains via sharing Q–Q edges, which consist of two $[TaQ_6]$ octahedral single chains by edge sharing of Q atoms (Figure 1c,d). The constituent units and the combination mode of two compounds are pretty close. However, their symmetry operations are different, making them in different space groups.

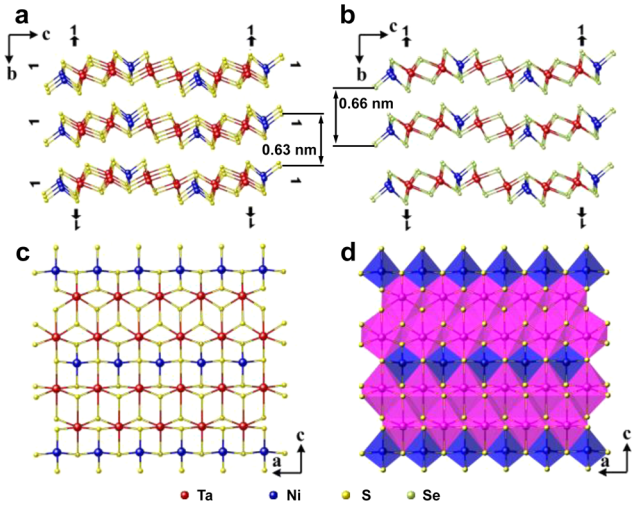

Figure 1. Crystal structure of layered Ta_2NiQ_5 (Q = S, Se). The structures of (a) Ta_2NiS_5 and (b) Ta_2NiSe_5 with 2_1 screw axis and 2 rotation axis viewed from the *a*-axis. (c) Projection of the layered structure of Ta_2NiS_5 along the *b*-axis. (d) The layered structure of Ta_2NiS_5 consisting of NiS_4 tetrahedra (blue) and TaS_6 octahatra (pink).

A 2-fold screw axis along the *c*-axis exists in the structure of Ta_2NiS_5, but not Ta_2NiSe_5, which can be attributed to the radius difference of Se^{2-} and S^{2-} anions (Figure 1a,b). In addition, the thickness of single-layer Ta_2NiS_5 and Ta_2NiSe_5 calculated from the structure are 0.63 and 0.66 nm, respectively (Figure 1a,b).[31]

The layered microsized crystalline flakes of Ta_2NiS_5 and Ta_2NiSe_5 were synthesized from their elementary powders via the chemical vapor transport technique (see the Experimental Section for details). The scanning electron microscopy (SEM) images confirmed that the layered Ta_2NiS_5 crystals in irregular shape with size of 5–30 μm were obtained (Figure 2a,b). The

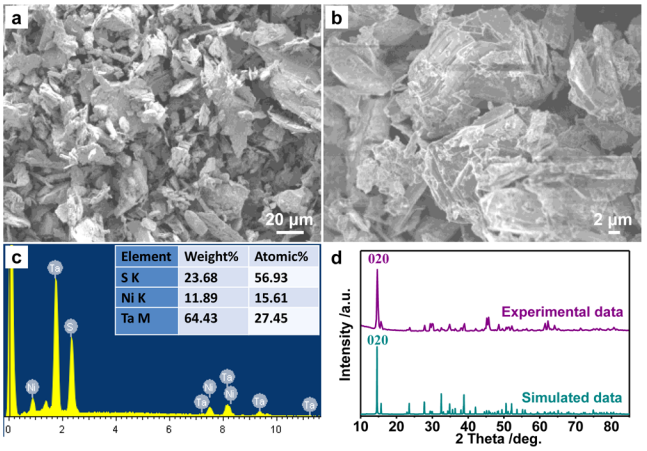

Figure 2. (a and b) SEM images and (c) EDS spectrum of Ta_2NiS_5 layered microflake. Inset in (c): The elemental ratio obtained from the EDS spectrum. (d) XRD pattern of Ta_2NiS_5 layered microflake.

energy-dispersive X-ray spectroscopy (EDS) spectrum gives strong signals of Ta, Ni and S (Figure 2c). All the peaks of the X-ray diffraction (XRD) pattern can be indexed to the simulated pattern of Ta_2NiS_5 crystal (Figure 2d), indicating the single-crystalline nature of the prepared Ta_2NiS_5 crystal. Similarly, the SEM images show that the layered Ta_2NiSe_5 crystals in flake-like structure with size of 20–500 μm were obtained (Figure 3a,b). Strong signals of Ta, Ni and Se were observed in its EDS spectrum (Figure 3c). All the peaks of the

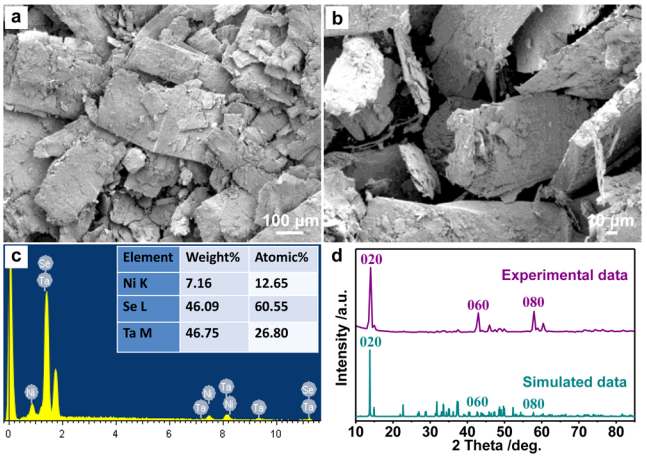

Figure 3. (a and b) SEM images and (c) EDS spectrum of Ta_2NiSe_5 layered microflake. Inset in (c): The elemental ratio obtained from the EDS spectrum. (d) XRD pattern of Ta_2NiSe_5 layered microflake.

DOI: 10.1021/jacs.5b06982
J. Am. Chem. Soc. 2015, 137, 10430–10436

experimental XRD pattern can be indexed to the simulated pattern of Ta_2NiSe_5 crystal (Figure 3d), indicating the single-crystalline nature of the prepared Ta_2NiSe_5 crystal. The obtained crystalline flakes of Ta_2NiS_5 and Ta_2NiSe_5 were then used for preparation of ultrathin 2D nanosheets via the electrochemical Li-intercalation and exfoliation method (see the Experimental Section for details).[29,30] The obtained ultrathin 2D nanosheets of Ta_2NiS_5 and Ta_2NiSe_5 were characterized by SEM, atomic force microscopy (AFM), transmission electron microscopy (TEM), EDS, X-ray photoelectron spectroscopy (XPS), and Raman spectroscopy.

Morphologies and chemical components of the exfoliated ultrathin 2D Ta_2NiS_5 nanosheets were characterized (Figure 4).

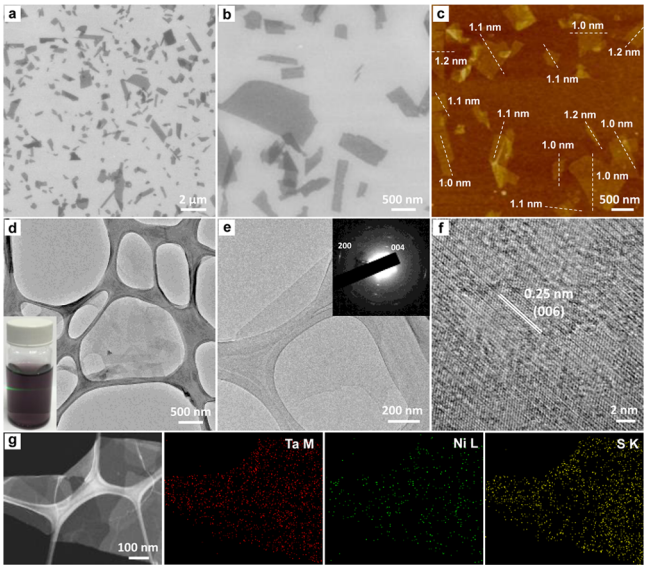

Figure 4. Characterization of single-layer Ta_2NiS_5 nanosheets. (a and b) SEM images and (c) AFM height image of single-layer Ta_2NiS_5 nanosheets. (d) Low-magnification TEM image of single-layer Ta_2NiS_5 nanosheets. Inset: Photograph of Tyndall effect of the Ta_2NiS_5 nanosheet suspension. (e) TEM image of a typical Ta_2NiS_5 nanosheet. Inset: The corresponding SAED pattern of Ta_2NiS_5 nanosheet with the electron beam perpendicular to its basal plane. (f) HRTEM image of a typical Ta_2NiS_5 nanosheet. (g) EDS elemental mapping of a typical Ta_2NiS_5 nanosheet.

The SEM images in Figure 4a,b show that Ta_2NiS_5 nanosheets with size ranging from tens of nanometers to few micrometers are well dispersed on the Si/SiO_2 substrate. AFM characterization confirmed that the thickness of Ta_2NiS_5 nanosheets is 1.1 ± 0.1 nm (Figure 4c, S1), confirming the single-layer Ta_2NiS_5 nanosheets were prepared. The production yield of single layer is ca. 86%. The low-magnification TEM image in Figure 4d gives a consistent result with the SEM images (Figure 4a, b). The solution of the as-exfoliated single-layer Ta_2NiS_5 nanosheet suspension shows a typical Tyndall effect when a green laser goes through it (inset in Figure 4d), confirming their colloidal structure. The TEM image in Figure 4e shows a typical single-layer Ta_2NiS_5 nanosheet with size of ~1 μm. The corresponding selected area electron diffraction (SAED) pattern gives clear bright spots, confirming its single-crystalline structure (inset in Figure 4e). Continuous lattice fringes can be clearly observed from the high-resolution TEM (HRTEM) image of a typical Ta_2NiS_5 nanosheet (Figure 4f), further confirming its single-crystalline nature. The measured lattice distance is about 0.25 nm, corresponding to the (006) planes of the Ta_2NiS_5 crystal. Furthermore, the elemental components of Ta_2NiS_5 nanosheets were confirmed by EDS and corresponding elemental mapping. The presence of Ta, Ni and S is evidenced by their strong signals in its EDS spectrum (Figure S2). The uniform distribution of Ta, Ni and S in the Ta_2NiS_5 nanosheet is evidenced by its corresponding elemental mapping (Figure 4g).

Moreover, XPS was used to characterize the elemental binding energies of obtained single-layer Ta_2NiS_5 nanosheets. The XPS survey spectrum gives intense signals of Ta, Ni, and S (Figure S3a). Three peaks at 24.1, 26.1, and 28.0 eV were detected in the high-resolution XPS spectrum of Ta 4f (Figure S3b). The two main peaks at 24.1 and 26.1 eV are assignable to the Ta $4f_{7/2}$ and Ta $4f_{5/2}$ of Ta^{4+} in Ta_2NiS_5, respectively.[32,33] The XPS spectrum of Ni 2p also gives three peaks located at 853.5, 856.2, and 861.3 eV, respectively (Figure S3c). The peak at 853.5 eV along with a satellite peak at 861.3 eV were fitted to the binding energies of Ni^{2+} in Ta_2NiS_5.[34] Two main peaks located at 161.5 and 162.7 eV were fitted as the dominant state of the XPS S spectrum (Figure S3d), which are assignable to the S^{2-} in Ta_2NiS_5.[33,34] In addition, Raman spectroscopy was also used to characterize the layered microflakes and single-layer nanosheets of Ta_2NiS_5. The Raman peaks of single-layer Ta_2NiS_5 nanosheets located at 126.6, 148.7, 293.2, 342.5, and 396.1 cm^{-1}, similar to that of layered microflakes of Ta_2NiS_5, although some peaks of single-layer Ta_2NiS_5 nanosheets showed small blue shift (Figure S4).

Besides Ta_2NiS_5 nanosheets, the Ta_2NiSe_5 nanosheets can also be prepared from its bulk crystal through the same method. The characterization of Ta_2NiSe_5 nanosheets is shown in Figure 5. The SEM image shows the sheet-like structure of exfoliated

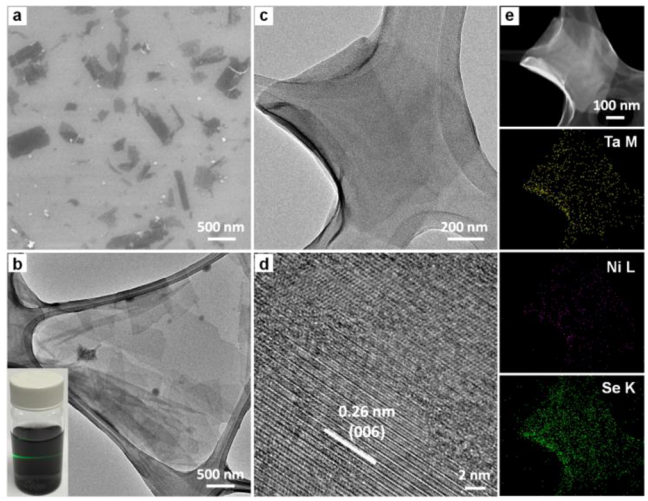

Figure 5. Characterization of few-layer Ta_2NiSe_5 nanosheets. (a) SEM image of Ta_2NiSe_5 nanosheets. (b) Low-magnification TEM image of Ta_2NiSe_5 nanosheets. Inset: Photograph of Tyndall effect of the Ta_2NiSe_5 nanosheet suspension. (c) TEM image of a typical Ta_2NiSe_5 nanosheet. (d) HRTEM image of a typical Ta_2NiSe_5 nanosheet. (e) EDS elemental mapping of a typical Ta_2NiSe_5 nanosheet.

Ta_2NiSe_5 (Figure 5a), which is further confirmed by the low-magnification TEM image (Figure 5b). The lateral size of Ta_2NiSe_5 nanosheets estimated from the SEM and TEM images ranges from tens of nanometers to 1 μm. The AFM measurement reveals that the thickness of Ta_2NiSe_5 nanosheets is in the range of 1.9−3.5 nm, suggesting its few-layer nature (2−5 layers) (Figure S5). A typical Tyndall effect was observed

DOI: 10.1021/jacs.5b06982
J. Am. Chem. Soc. 2015, 137, 10430−10436

when a green laser goes through the solution of Ta_2NiSe_5 nanosheets (inset in Figure 5b), confirming their colloidal structure. Figure 5c shows TEM image of a typical Ta_2NiSe_5 nanosheet with size of ~1 μm. The HRTEM image of a typical Ta_2NiSe_5 nanosheet reveals its single-crystalline nature with a lattice spacing of ~0.26 nm (Figure 5d), assignable to the (006) planes of Ta_2NiSe_5 crystal. The EDS spectrum of a typical Ta_2NiSe_5 nanosheet gives strong signals of Ta, Ni and Se (Figure S6), indicating the presence of Ta, Ni and Se in the nanosheets. Its corresponding elemental mapping reveals the homogeneous distribution of the Ta, Ni and Se elements in the obtained Ta_2NiSe_5 nanosheet (Figure 5e).

Moreover, the few-layer Ta_2NiSe_5 nanosheets were also characterized by XPS. The XPS survey spectrum of Ta_2NiSe_5 nanosheets gives obvious signals of Ta, Ni and Se (Figure S7a). Two main peaks located at 23.7 and 25.7 eV were fitted as the dominant states in the high-resolution Ta 4f spectrum (Figure S7b), assignable to the Ta^{4+} of Ta_2NiSe_5.[35] The peaks of Ni 2p located at binding energy of 853.3 and 861.6 eV can be indexed to the binding energies of Ni^{2+} in Ta_2NiSe_5 (Figure S7c).[35] Three peaks located at 53.8, 54.7, and 55.7 eV were fitted as the dominant states of the Se 3d spectrum (Figure S7d), which are assignable to the Se^{2-} in Ta_2NiSe_5.[35]

The development of sensors for detection of biomolecules simply, rapidly, and selectively is of great importance in the fields of clinical diagnostics, gene profiling, and environmental monitoring.[36−40] Previous studies have proven that ultrathin 2D nanosheets, such as graphene oxides (GO) and graphitic carbon nitride ($g\text{-}C_3N_4$), could be appealing candidates for construction of fluorescent sensors for DNA detection.[41−49] Recently, our group first demonstrated that single-layer MoS_2, TaS_2 and TiS_2 nanosheets can be used as sensing platforms for the detection of DNA, based on their different fluorescence-quenching abilities toward the single-stranded (ss) and double-stranded (ds) DNA.[14,15] In this work, as a proof-of-concept application, the single-layer Ta_2NiS_5 nanosheet is used as a novel sensing platform for detection of DNA. The proposed strategy for this assay is shown in Figure 6a. The fluorescence quenching ability of single-layer Ta_2NiS_5 nanosheets was first evaluated. The dye-labeled ssDNA was mixed with the single-layer Ta_2NiS_5 nanosheets. The sequences of the Texas red-labeled ssDNA probe (P) and the target DNA (T) used in this study are listed in Table S1. As shown in Figure 6b, P showed strong fluorescence emission in the absence of Ta_2NiS_5 nanosheets (pink curve). After addition of single-layer Ta_2NiS_5 nanosheets with final concentration of 4.0 μg mL^{-1} (Figure 7a), the fluorescence intensity was quenched within 10 min (black curve (P + Ta_2NiS_5) and inset in Figure 6b). This result indicated that the interaction between the single-layer Ta_2NiS_5 nanosheet and ssDNA is strong, and the fluorescence quenching ability of Ta_2NiS_5 is very high. It was found that when P was hybridized with an equal amount of T, the dsDNA (P/T duplex) was formed and the quenched fluorescence of P in the presence of Ta_2NiS_5 was recovered (red curve (P/T + Ta_2NiS_5) in Figure 6b). Note that the fluorescence intensity of P/T duplex at 610 nm is approximately 82% of that of P in the absence of single-layer Ta_2NiS_5 nanosheets (blue curve (P/T) in Figure 6b), which is due to the different effect of the primary and secondary structures of DNA on the fluorescence properties of labeled dyes.[50] These results indicate that single-layer Ta_2NiS_5 nanosheets possess much weaker interaction with dsDNA compared to ssDNA, which is similar to our previous work.[14,15]

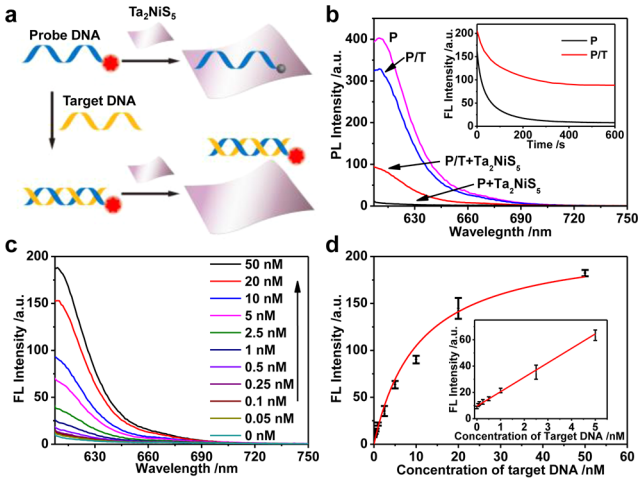

Figure 6. Single-layer Ta_2NiS_5 nanosheet-based fluorescence sensor for DNA detection. (a) Schematic illustration of the DNA detection based on single-layer Ta_2NiS_5 nanosheets. (b) Fluorescence spectra of P (10 nM) and P/T (10 nM) in the absence and presence of single-layer Ta_2NiS_5 nanosheets. Inset: The fluorescence quenching curves of P and P/T in the presence of single-layer Ta_2NiS_5 nanosheet (4.0 μg mL^{-1}). (c) Fluorescence spectra of P in the presence of different concentrations of T (0, 0.05, 0.1, 0.25, 0.5, 1, 2.5, 5, 10, 20, 50 nM) with addition of single-layer Ta_2NiS_5 nanosheet (4.0 μg mL^{-1}). (d) Calibration curve of DNA detection. Inset: The linear plot of fluorescence peak intensity of P vs the concentration of T with addition of single-layer Ta_2NiS_5 nanosheet (4.0 μg mL^{-1}). The excitation and emission wavelengths are 596 and 610 nm, respectively.

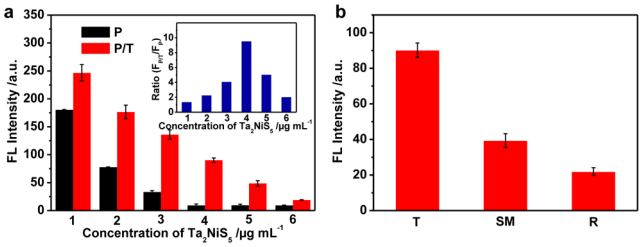

Figure 7. (a) Fluorescence intensity of P + Ta_2NiS_5 (black) and P/T + Ta_2NiS_5 (red) in the presence of single-layer Ta_2NiS_5 nanosheets at different final concentration of 1.0, 2.0, 3.0, 4.0, 5.0, and 6.0 μg mL^{-1} (P, 10 nM; T, 10 nM). The error bars represent standard deviation of three parallel experiments. Inset: The fluorescence intensity ratio ($F_{P/T}/F_P$) at 610 nm in the presence of single-layer Ta_2NiS_5 nanosheets with different final concentration of 1.0, 2.0, 3.0, 4.0, 5.0, and 6.0 μg mL^{-1} (P, 10 nM; T, 10 nM). (b) Selectivity of the single-layer Ta_2NiS_5 nanosheet-based sensor in the presence of complementary target DNA (T), single-base mismatched DNA (SM), and random DNA (R). The excitation and emission wavelengths are 596 and 610 nm, respectively.

On the basis of the aforementioned results, the single-layer Ta_2NiS_5 nanosheet can serve as a novel platform of fluorescent sensor for quantitative detection of DNA. Different concentrations of T (0−50 nM) were hybridized with P (10 nM) at room temperature, followed with the addition of single-layer Ta_2NiS_5 nanosheets with a final concentration of 4.0 μg mL^{-1}. The mixture was incubated for 10 min prior to the fluorescence measurements. The recovery of fluorescence intensity of P can be obviously observed with the concentration of T in addition of single-layer Ta_2NiS_5 nanosheet (final concentration: 4.0 μg mL^{-1}) (Figure 6c,d). A linear relationship in the range of 0−5 nM was observed and a detection limit of 50 pM is achieved

DOI: 10.1021/jacs.5b06982
J. Am. Chem. Soc. 2015, 137, 10430−10436

Table 1. Comparison of Fluorescent DNA Sensors

materials	fluorescent reporter[a]	sensitivity (detection limit)	detection time	comments	ref
GO	FAM, ROX, Cy5	100 pM	1 min	Multiplexed analysis	41
GO	FAM	2 nM	5 min	-	42
GO	Silver nanoclusters	0.5 nM	1−1.5 h	Multiplexed analysis	43
GO	FITC	6.25 pM	20 min	-	44
GO	SYBR Green I	0.25 pM	5 min	DNA intercalating dye	45
GO	Graphene quantum dots	75 pM	30 min	-	46
GO	FAM	0.2 nM	20 s	-	47
GO	FAM, ROX	5 pM	90 min	Exonuclease III amplification	48
g-C_3N_4	FAM, ROX	81 pM	30 min	Exonuclease III amplification	49
MoS_2	FAM	0.5 nM	5 min	-	14
TiS_2	FAM, Texas red	0.2 nM	5 min	Multiplexed analysis	15
TaS_2	FAM, Texas red	50 pM	5 min	Multiplexed analysis	15
Ta_2NiS_5	Texas red	50 pM	10 min	-	This work

[a]Abbreviations: FAM, carboxyfluorescein; ROX, 6-carboxyl-x-rhodamine; Cy5, cyanine 5; FITC, fluorescein isothiocyanate.

(inset in Figure 6d), which is much lower than that of single-layer MoS_2-based DNA sensor (0.5 nM).[14] It is also comparable with the single-layer TaS_2-based DNA sensor (50 pM).[15] The comparison of our work with the reported fluorescent DNA sensors based on other 2D nanomaterials is shown in Table 1.[14,15,40−49] More importantly, as shown in Figure 7b, the single-base mismatched DNA (SM) and random DNA (R) did not cause the distinct increase of fluorescent signal compared with the complementary target DNA (T), demonstrating our single-layer Ta_2NiS_5 nanosheet-based fluorescent sensor possesses excellent selectivity, which may hold great promise for the real sample analysis.

CONCLUSIONS

In summary, we have successfully prepared ultrathin 2D ternary chalcogenide nanosheets including Ta_2NiS_5 and Ta_2NiSe_5 in high-yield and large-scale in solution by exfoliation of their layered microflakes. To the best of our knowledge, this is the first report on the preparation of single-layer or few-layer ternary chalcogenide nanosheets in solution. Significantly, the single-layer Ta_2NiS_5 nanosheets with yield of ca. 86% were obtained. Due to its high fluorescence quenching ability, a novel fluorescent sensor for detection of DNA was developed based on the single-layer Ta_2NiS_5 nanosheets, showing excellent selectivity and sensitivity with detection limit of 50 pM, which is better than that of the single-layer MoS_2-based biosensor. This highly selective and sensitive biosensor might be used for the real sample analysis in the near future.

EXPERIMENTAL SECTION

Chemicals. Tantalum powder (99.9%), nickel powder (99.9%), sulfur powder (99.995%), selenium powder (99.995%), phosphate buffer saline (PBS) tablets, acetone, and *N*-methylpyrrolidone (NMP) were purchased from Sigma-Aldrich (Germany). Lithium-ion battery electrolyte, i.e., 1 M of $LiPF_6$ dissolved in a mixture of ethyl carbonate (EC) and dimethyl carbonate (DMC) (v/v = 1:1), was purchased from Charslton Technologies Pte Ltd. (Singapore). Poly(vinylidene fluoride) (PVDF), lithium foil, and copper foil were purchased from the ACME Research Support Pte Ltd. (Singapore). All the DNA sequences used in this study were synthesized and purified by Shanghai Sangon Biotechnology Co. (China). PBS tablets were dissolved in water to prepare PBS solution (0.01 M, pH 7.4). All the chemicals were used as received without further purification. The Milli-Q water (Milli-Q System, Millipore) was used in all experiments.

Preparation of Layered Bulk Crystals of Ta_2NiS_5 and Ta_2NiSe_5. Bulk crystals of Ta_2NiS_5 and Ta_2NiSe_5 were prepared by the chemical vapor transport method with iodide as the transporting agency. The stoichiometric amounts with the molar ratio of Ta:Ni:S (or Se) = 2:1:5 of high purity Ta, Ni and S (or Se) with the total weight of 1 g, i.e., 574.8 mg of Ta, 110.2 mg of Ni, and 315.0 mg of S for Ta_2NiS_5, or 424.4 mg of Ta, 81.4 mg of Ni, and 494.2 mg of Se for Ta_2NiSe_5, mixed with 40 mg iodide were sealed in an evacuated 20 cm-long quartz tube under vacuum of 10^{-6} Torr. The sealed tube was placed in a three-zone furnace. The reaction zone was prereacted at 850 °C for 30 h, while the grown zone was kept at 900 °C. The temperature of reaction zone was then increased to 1030 °C at increasing rate of 10 °C/min, while the growth zone kept at 900 °C for 4 days in order to grow the single crystals of Ta_2NiS_5 or Ta_2NiSe_5. Finally, the furnace was naturally cooled down to room temperature and the single crystals of Ta_2NiS_5 or Ta_2NiSe_5 were collected in the growth zone. The obtained big single crystals were ground into microflakes for the SEM and XRD characterizations. The layered microflakes were further used as the raw materials for preparation of ultrathin two-dimensional (2D) nanosheets.

Preparation of Ta_2NiS_5 and Ta_2NiSe_5 Nanosheets. The ultrathin Ta_2NiS_5 and Ta_2NiSe_5 nanosheets were prepared from their layered microflakes by using the electrochemcial Li-intercalaction and exfoliation method, which was developed by our group recently for preparation of single-layer or few-layer transition metal dichachogenide (TMD) nanosheets (e.g., MoS_2, TiS_2, TaS_2, and WS_2).[29,30] The powders of Ta_2NiS_5 or Ta_2NiSe_5 layered crystalline microflakes, PVDF, and acetylene black with the mass ratio of 8:1:1 were mixed in NMP to form a homogeneous slurry, which was then uniformly coated onto a copper foil disc. After a drying step, the copper foil disc coated with Ta_2NiS_5 or Ta_2NiSe_5 crystals was assembled in a battery cell as the cathode, in which the Li foil and 1 M of $LiPF_6$ were used as the anode and electrolyte, respectively. The lithium intercalation in the layered crystalline microflakes was performed during the discharge process. After that, the electrode was taken out from the battery cell and washed with acetone, followed by sonication in water. The obtained suspension was centrifuged and washed with water to get the final product, i.e., Ta_2NiS_5 or Ta_2NiSe_5 nanosheets, which were collected for further characterization and experimental usage.

Characterization. A drop of solution containing the prepared nanosheets was placed on a holey carbon-coated copper grid and Si/SiO_2 substrate, and then naturally dried in air prior to characterization. A transmission electron microscope (JEOL JEM-2100F) coupled with energy dispersive X-ray spectroscopy (EDS) was used to take the transmission electron microscopy (TEM) images, EDS spectra and elemental mappings. A Dimension 3100 AFM with Nanoscope IIIa controller (Veeco, Fremont, CA) was used to record atomic force microscope (AFM) images in tapping mode under ambient conditions. The powder X-ray diffraction (XRD) patterns were recorded on a Bruker D8 diffractometer (German) with a Cu Kα (λ = 1.54178 Å) X-ray source. X-ray photoelectron spectroscopy (XPS)

DOI: 10.1021/jacs.5b06982
J. Am. Chem. Soc. 2015, 137, 10430−10436

was recorded on a VG ESCALAB 220i-XL instrument (base pressure $<5 \times 10^{-10}$ mbar) equipped with a monochromatic Al Kα (1486.7 eV) X-ray source. The Raman spectra was measured on A WITec CRM200 confocal Raman microscopy system with the excitation line of 532 nm and air cooling charge coupled device as the detector (WITec Instruments Corp, Germany). The Raman band of a silicon wafer at 520 cm^{-1} was used as the reference to calibrate the spectrometer. Fluorescence measurements were carried out on a Shimadzu RF-5301 PC instrument with an Xe-lamp light source.

DNA Detection. In a typical hybridization process, 10 μL of probe (P, 1 μM) was hybridized with 10 μL of target DNA (T, 0−5 μM) in 972 μL of PBS solution (0.01 M, pH 7.4) for 30 min. Then, 8 μL of Ta_2NiS_5 nanosheet solution (0.5 mg mL^{-1}) was added into the aforementioned mixture, which was incubated for 10 min prior to the fluorescence measurements. The hybridization process was done at different final concentration of T (0−50 nM). The excitation and emission wavelengths were 596 and 610 nm, respectively. To get the optimal concentration of single-layer Ta_2NiS_5 nanosheets used in fluorescence sensors, the fluorescence intensity changes of P and P/T (P, 10 nM; T, 10 nM) were studied in the presence of Ta_2NiS_5 at different final concentration (1.0, 2.0, 3.0, 4.0, 5.0, and 6.0 μg mL^{-1}) (Figure 7a). We found that the single-layer Ta_2NiS_5 nanosheet with final concentration of 4.0 μg mL^{-1} exhibited the highest signal-to-noise ratio (Figure 7a), which was the optimized concentration for the DNA detection.

To study the selectivity of single-layer Ta_2NiS_5 nanosheet-based sensors, 10 μL of probe (P, 1 μM) was hybridized with 10 μL of target DNA (T, 1 μM), 10 μL of single-base mismatch DNA (SM, 1 μM), and 10 μL of random DNA (R, 1 μM), separately, in 972 μL of PBS solution (0.01 M, pH 7.4) for 30 min (Figure 7b). Then, the single-layer Ta_2NiS_5 nanosheet solution (8 μL, 0.5 mg mL^{-1}) was added into the aforementioned mixtures, which were incubated for 10 min. After that, the hybridization processes were monitored by fluorescence measurements at the final concentrations of T (10 nM), SM (10 nM), and R (10 nM), respectively.

■ ASSOCIATED CONTENT

Supporting Information

The Supporting Information is available free of charge on the ACS Publications website at DOI: 10.1021/jacs.5b06982.

EDS, AFM, Raman, and XPS data of ternary chalcogenide nanosheets; data of the used DNA sequences (PDF)

■ AUTHOR INFORMATION

Corresponding Authors

*hzhang@ntu.edu.sg

*z.liu@ntu.edu.sg

*iamlhwang@njupt.edu.cn

Author Contributions

⊥These authors contributed equally to this work.

Notes

The authors declare no competing financial interest.

■ ACKNOWLEDGMENTS

This work was supported by MOE under AcRF Tier 2 (No. MOE2013-T2-1-034; ARC 19/15, No. MOE2014-T2-2-093) and AcRF Tier 1 (RGT18/13, RG5/13), NTU under Start-Up Grant (M4081296.070.500000) and iFood Research Grant (M4081458.070.500000), and Singapore Millennium Foundation in Singapore. This Research is also conducted by NTU-HUJ-BGU Nanomaterials for Energy and Water Management Programme under the Campus for Research Excellence and Technological Enterprise (CREATE), that is supported by the National Research Foundation, Prime Minister's Office, Singapore. This work is also supported by the Singapore National Research Foundation under NRF RF Award No. NRF-RF2013−08, the start-up funding from Nanyang Technological University (M4081137.070) and AcRF Tier 1 (RG 10/14).

■ REFERENCES

(1) Nicolosi, V.; Chhowalla, M.; Kanatzidis, M. G.; Strano, M. S.; Coleman, J. N. *Science* **2013**, *340*, 1226419.

(2) Huang, X.; Zeng, Z. Y.; Zhang, H. *Chem. Soc. Rev.* **2013**, *42*, 1934−1946.

(3) Wang, Q. H.; Kalantar-Zadeh, K.; Kis, A.; Coleman, J. N.; Strano, M. S. *Nat. Nanotechnol.* **2012**, *7*, 699−712.

(4) Xu, M. S.; Liang, T.; Shi, M. M.; Chen, H. Z. *Chem. Rev.* **2013**, *113*, 3766−3798.

(5) Tan, C. L.; Zhang, H. *Chem. Soc. Rev.* **2015**, *44*, 2713−2731.

(6) Radisavljevic, B.; Radenovic, A.; Brivio, J.; Giacometti, V.; Kis, A. *Nat. Nanotechnol.* **2011**, *6*, 147−150.

(7) Yin, Z. Y.; Li, H.; Li, H.; Jiang, L.; Shi, Y. M.; Sun, Y. H.; Lu, G.; Zhang, Q.; Chen, X. D.; Zhang, H. *ACS Nano* **2012**, *6*, 74−80.

(8) Wu, W. Z.; Wang, L.; Li, Y. L.; Zhang, F.; Lin, L.; Niu, S. M.; Chenet, D.; Zhang, X.; Hao, Y. F.; Heinz, T. F.; Hone, J.; Wang, Z. L. *Nature* **2014**, *514*, 470−474.

(9) Li, H.; Wu, J.; Yin, Z. Y.; Zhang, H. *Acc. Chem. Res.* **2014**, *47*, 1067−1075.

(10) Tan, C. L.; Liu, Z. D.; Huang, W.; Zhang, H. *Chem. Soc. Rev.* **2015**, *44*, 2615−2628.

(11) Voiry, D.; Yamaguchi, H.; Li, J. W.; Silva, R.; Alves, D. C. B.; Fujita, T.; Chen, M. W.; Asefa, T.; Shenoy, V. B.; Eda, G.; Chhowalla, M. *Nat. Mater.* **2013**, *12*, 850−855.

(12) Xie, J. F.; Zhang, J. J.; Li, S.; Grote, F.; Zhang, X. D.; Zhang, H.; Wang, R. X.; Lei, Y.; Pan, B. C.; Xie, Y. *J. Am. Chem. Soc.* **2013**, *135*, 17881−17888.

(13) Huang, X.; Zeng, Z. Y.; Bao, S. Y.; Wang, M. F.; Qi, X. Y.; Fan, Z. X.; Zhang, H. *Nat. Commun.* **2013**, *4*, 1444.

(14) Zhu, C. F.; Zeng, Z. Y.; Li, H.; Li, F.; Fan, C. H.; Zhang, H. *J. Am. Chem. Soc.* **2013**, *135*, 5998−6001.

(15) Zhang, Y.; Zheng, B.; Zhu, C. F.; Zhang, X.; Tan, C. L.; Li, H.; Chen, B.; Yang, J.; Chen, J. Z.; Huang, Y.; Wang, L. H.; Zhang, H. *Adv. Mater.* **2015**, *27*, 935−939.

(16) Perkins, F. K.; Friedman, A. L.; Cobas, E.; Campbell, P. M.; Jernigan, G. G.; Jonker, B. T. *Nano Lett.* **2013**, *13*, 668−673.

(17) Wu, S. X.; Zeng, Z. Y.; He, Q. Y.; Wang, Z. J.; Wang, S. J.; Du, Y. P.; Yin, Z. Y.; Sun, X. P.; Chen, W.; Zhang, H. *Small* **2012**, *8*, 2264−2270.

(18) Acerce, M.; Voiry, D.; Chhowalla, M. *Nat. Nanotechnol.* **2015**, *10*, 313−318.

(19) Sun, Y. F.; Gao, S.; Xie, Y. *Chem. Soc. Rev.* **2014**, *43*, 530−546.

(20) Sun, G. Z.; Liu, J. Q.; Zhang, X.; Wang, X. W.; Li, H.; Yu, Y.; Huang, W.; Zhang, H.; Chen, P. *Angew. Chem., Int. Ed.* **2014**, *53*, 12576−12580.

(21) Cheng, L.; Liu, J. J.; Gu, X.; Gong, H.; Shi, X. Z.; Liu, T.; Wang, C.; Wang, X. Y.; Liu, G.; Xing, H. Y.; Bu, W. B.; Sun, B. Q.; Liu, Z. *Adv. Mater.* **2014**, *26*, 1886−1893.

(22) Chen, Y.; Tan, C. L.; Zhang, H.; Wang, L. Z. *Chem. Soc. Rev.* **2015**, *44*, 2681−2701.

(23) Novoselov, K. S.; Jiang, D.; Schedin, F.; Booth, T. J.; Khotkevich, V. V.; Morozov, S. V.; Geim, A. K. *Proc. Natl. Acad. Sci. U. S. A.* **2005**, *102*, 10451−10453.

(24) Coleman, J. N.; Lotya, M.; O'Neill, A.; Bergin, S. D.; King, P. J.; Khan, U.; Young, K.; Gaucher, A.; De, S.; Smith, R. J.; Shvets, I. V.; Arora, S. K.; Stanton, G.; Kim, H. Y.; Lee, K.; Kim, T. G.; Duesberg, G. S.; Hallam, T.; Boland, J. J.; Wang, J. J.; Donegan, J. F.; Grunlan, J. C.; Moriarty, G.; Shmeliov, A.; Nicholls, R. J.; Perkins, J. M.; Grieveson, E. M.; Theuwissen, K.; McComb, D. W.; Nellist, P. D.; Nicolosi, V. *Science* **2011**, *331*, 568.

(25) Smith, R. J.; King, P. J.; Lotya, M.; Wirtz, C.; Khan, U.; De, S.; O'Neill, A.; Duesberg, G. S.; Grunlan, J. C.; Moriarty, G.; Chen, J.;

Wang, J. Z.; Minett, A. I.; Nicolosi, V.; Coleman, J. N. *Adv. Mater.* **2011**, *23*, 3944−3948.
(26) Guan, G.; Zhang, S.; Liu, S.; Cai, Y.; Low, M.; Teng, C. P.; Phang, I. Y.; Cheng, Y.; Duei, K. L.; Srinivasan, B. M.; Zheng, Y.; Zhang, Y. W.; Han, M. Y. *J. Am. Chem. Soc.* **2015**, *137*, 6152−6155.
(27) Dines, M. B. *Mater. Res. Bull.* **1975**, *10*, 287−291.
(28) Zheng, J.; Zhang, H.; Dong, S. H.; Liu, Y. P.; Nai, C. T.; Shin, H. S.; Jeong, H. Y.; Liu, B.; Loh, K. P. *Nat. Commun.* **2014**, *5*, 2995.
(29) Zeng, Z. Y.; Yin, Z. Y.; Huang, X.; Li, H.; He, Q. Y.; Lu, G.; Boey, F.; Zhang, H. *Angew. Chem., Int. Ed.* **2011**, *50*, 11093−11097.
(30) Zeng, Z. Y.; Sun, T.; Zhu, J. X.; Huang, X.; Yin, Z. Y.; Lu, G.; Fan, Z. X.; Yan, Q. Y.; Hng, H. H.; Zhang, H. *Angew. Chem., Int. Ed.* **2012**, *51*, 9052−9056.
(31) Sunshine, S. A.; Ibers, J. A. *Inorg. Chem.* **1985**, *24*, 3611−3614.
(32) Crawack, H. J.; Pettenkofer, C. *Solid State Commun.* **2001**, *118*, 325−332.
(33) Scharli, M.; Brunner, J. *Solid State Commun.* **1983**, *45*, 305−307.
(34) Legrand, D. L.; Nesbitt, H. W.; Bancroft, G. M. *Am. Mineral.* **1998**, *83*, 1256−1265.
(35) Wakisaka, Y.; Sudayama, T.; Takubo, K.; Mizokawa, T.; Arita, M.; Namatame, H.; Taniguchi, M.; Katayama, N.; Nohara, M.; Takagi, H. *Phys. Rev. Lett.* **2009**, *103*, 026402.
(36) Heller, M. J. *Annu. Rev. Biomed. Eng.* **2002**, *4*, 129−153.
(37) Tian, J.; Cheng, N.; Liu, Q.; Xing, W.; Sun, X. *Angew. Chem., Int. Ed.* **2015**, *54*, 5493−5497.
(38) Wang, L.; Zhang, Y.; Tian, J.; Li, H.; Sun, X. *Nucleic Acids Res.* **2011**, *39*, e37−e42.
(39) Li, H.; Zhang, Y.; Luo, Y.; Sun, X. *Small* **2011**, *7*, 1562−1568.
(40) Tian, J.; Liu, Q.; Shi, J.; Hu, J.; Asiri, A. M.; Sun, X.; He, Y. *Biosens. Bioelectron.* **2015**, *71*, 1−6.
(41) He, S.; Song, B.; Li, D.; Zhu, C.; Qi, W.; Wen, Y.; Wang, L.; Song, S.; Fang, H.; Fan, C. *Adv. Funct. Mater.* **2010**, *20*, 453−459.
(42) Lu, C. H.; Yang, H. H.; Zhu, C. L.; Chen, X.; Chen, G. N. *Angew. Chem., Int. Ed.* **2009**, *48*, 4785−4787.
(43) Liu, X.; Wang, F.; Aizen, R.; Yehezkeli, O.; Willner, I. *J. Am. Chem. Soc.* **2013**, *135*, 11832−11839.
(44) Pang, S.; Gao, Y.; Li, Y.; Liu, S.; Su, X. *Analyst* **2013**, *138*, 2749−2754.
(45) Li, J.; Huang, Y.; Wang, D.; Song, B.; Li, Z.; Song, S.; Wang, L.; Jiang, B.; Zhao, X.; Yan, J.; Liu, R.; He, D.; Fan, C. *Chem. Commun.* **2013**, *49*, 3125−3127.
(46) Qian, Z. S.; Shan, X. Y.; Chai, L. J.; Ma, J. J.; Chen, J. R.; Feng, H. *Nanoscale* **2014**, *6*, 5671−5674.
(47) Li, F.; Pei, H.; Wang, L.; Lu, J.; Gao, J.; Jiang, B.; Zhao, X.; Fan, C. *Adv. Funct. Mater.* **2013**, *23*, 4140−4148.
(48) Liu, X.; Aizen, R.; Freeman, R.; Yehezkeli, O.; Willner, I. *ACS Nano* **2012**, *6*, 3553−3563.
(49) Wang, Q.; Wang, W.; Lei, J.; Xu, N.; Gao, F.; Ju, H. *Anal. Chem.* **2013**, *85*, 12182−12188.
(50) Nazarenko, I.; Pires, R.; Lowe, B.; Obaidy, M.; Rashtchian, A. *Nucleic Acids Res.* **2002**, *30*, 2089−2195.

DOI: 10.1021/jacs.5b06982
J. Am. Chem. Soc. 2015, 137, 10430−10436